International Journal of Electrical, Electronic and Communication Sciences
ISSN: 2517-9438
Vol:9, No:11, 2015

High Performance Direct Torque Control for Induction Motor Drive Fed from Photovoltaic System

E. E. El-Kholy, Ahamed Kalas, Mahmoud Fauzy, M. El-Shahat Dessouki, Abdou. M. El-Refay, Mohammed El-Zefery

***Abstract*—**Direct Torque Control (DTC) is an AC drive control method especially designed to provide fast and robust responses. In this paper a progressive algorithm for direct torque control of three-phase induction drive system supplied by photovoltaic arrays using voltage source inverter to control motor torque and flux with maximum power point tracking at different level of insolation is presented. Experimental results of the new DTC method obtained by an experimental rapid prototype system for drives are presented. Simulation and experimental results confirm that the proposed system gives quick, robust torque and speed responses at constant switching frequencies.

***Keywords*—**Photovoltaic (PV) array, direct torque control (DTC), constant switching frequency, induction motor, maximum power point tracking (MPPT).

I. Introduction

IN present, energy decreases and tend to be more expensive. Therefore, renewable energy is an alternative choice. Especially, solar energy is widely used. PV is popular used because of clean energy, without pollution of environment, no danger for human and long life of using [1], [2].

To use the solar module effectively it is important to match the load to draw the maximum power at given solar irradiance level and temperature. Controlled DC-DC converters (boost-buck-buck/boost) are used ensure source load matching. An operating point of the module can be shifted by changing the duty ratio using MPPT. Several techniques like Perturb and observe (P&O), incremental conductance technique, fuzzy logic control, and artificial neural network have been presented [3]-[8]. PV system is always used in two applications. One is electrical generation in rural area and two is water pump system which is used in water treatment system and irrigation system in agriculture. The mostly used ones are water pump systems which are supplied by PV array use DC motor because they can be coupled directly to the PV array. However, the disadvantages of DC motor are expensive and high maintenance cost, therefore induction motor has replaced it [9]-[15].

In the beginning, several strategies for adjustable speed drives have been introduced like field oriented control, direct self-control (DSC) and DTC based space vector modulation [16]-[22]. Simplicity, high dynamic performance, quick torque response, as well as the fact that there is no need for co-ordinate transformation, voltage, or current decoupling and no need for an encoder are several advantages for DTC leading to remarkable commercial applications.

In this paper, a boost DC-DC converter using a power MOSFT as switching device is used [23]-[25]. A hybrid hysteresis current control with incremental conductance technique for MPPT is proposed. The torque and flux controller design for the overall DTC for induction motor has been investigated. The realization of excellent dynamic torque and flux response is presented.

E. E. EL-Kholy is with the Electrical Engineering Department, Faculty of Engineering, Menofiya University, Egypt, (e-mail: olwieissa@yahoo.com).

Ahamed Kalas and Mahmoud Fauzy are with the Electrical Engineering Department, Faculty of Engineering, Port Said University, Egypt.

M. El-Shahat Dessouki is with the Electrical Engineering Department, Faculty of Engineering, Port Said University, Egypt and King Abdul Aziz University, Faculty of Engineering, Electrical Engineering Department, Rabigh, Saudi Arabia, (e-mail: Dessouky_m@yahoo.com).

Abdou. M. El-Refay and Mohammed El-Zefery are with the Ministry of Communication, Kuwait (e-mail: m.aldhfiri@yahoo.com).

II. PV Module

A practical PV array consists of a collection of solar cells connected in series and/or parallel. An equivalent circuit model for a solar cell is shown in Fig. 1, it is derived as the key element is the current source generating the photovoltaic current (I_{pv}). The model consists of a current source (I_{source}), a diode, shunt resistor R_p and a series resistance (R_s) [28].

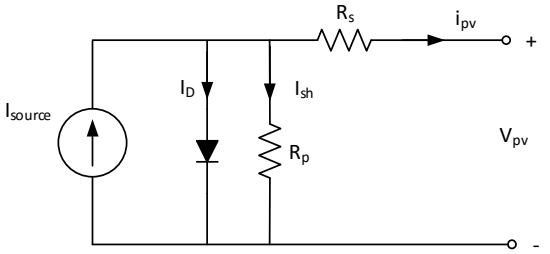

Fig. 1 PV model

The short circuit current (I_{sc}) is a function of the incident solar irradiance and the cell temperature as [28]:

$$I_{sc}\,(T_{ak}) = I_{sc}(T_{rk}) * (1.0 + A[T_{ak} - T_{rk}]) \quad (1)$$

$$I_{sc}\,(\mathrm{G}) = \frac{G}{G_0} I_{sc}(G_0) \quad (2)$$

where; T_{rk}: rated temperature in Kelvin; T_{ak}: module temperature in Kelvin; I_{sc}: short circuit current per cell; A: temperature coefficient of I_{sc}; G: irradiance; G_0: normal value of irradiance 1kw/m^2.

The thermal voltages (V_{th}) at rated temperature and module temperature are [28];

$$V_{th}(T_{rk}) = \frac{nk}{q} T_{rk} \quad (3)$$

$$V_{th}(T_{ak}) = \frac{nk}{q} T_{ak} \quad (4)$$

The saturation currents (I_{sat}) at rated temperature and module temperature are [28];

$$I_{Sat.}(T_{rk}) = \frac{I_{SC}(T_{rk})}{\left(e^{\left(\frac{V_{OC}(T_{rk})}{V_{th}(T_{rk})}\right)} - 1\right)} \quad (5)$$

$$I_{sat.}(T_{ak}) = \left[I_{sat.}(T_{rk}) * \left(\frac{T_{ak}}{T_{rk}}\right)^{\frac{3}{n}}\right] * e^{\left(-b*\left(\frac{1}{T_{ak}} - \frac{1}{T_{rk}}\right)\right)} \quad (6)$$

$$b = E_g * \frac{q}{N * K} \quad (7)$$

where; N: Identity factor; K: Boltzman constant; q: electron charge (=1.602e-19); E: band gap energy.

The PV current at rated temperature is [28];

$$i_{PV}(T_{rk}) = I_{SC}(T_{rk}) - I_{sat}(T_{rk}) * \left[e^{\frac{q}{NKT_{rk}}(V_{PV}(T_{rk}) + i_{PV}(T_{rk}) * R_s)} - 1\right] \quad (8)$$

where: R_s : series resistance; I_{pv}: module current; V_{pv}: module voltage.

III. Boost Converter

The topology of boost converter is shown in Fig. 2. For this converter the output voltage is always higher than the input PV voltage. Power flow is controlled by means of the on/off duty cycle of the switching transistor. This converter topology can be used in conjunction with lower PV voltages. No extra blocking diode is necessary when the boost topology is used [25]-[27].

The boost converter is described by three modes of operation, on or off. When the switch S is on (Pattern I), the energy from the PV is stored in the inductor L_1. When the switch S is off (Pattern II), the energy is delivered to the capacitor C. The Pattern (I), of the boost converter can be expressed by the following equations (S is on and D is off) [25];

$$V_{PV} = i_{PV} r_1 + L_1 \frac{di_{PV}}{dt} \quad (9)$$

$$i_c = c_o \frac{dE_{DC}}{dt} \quad (10)$$

$$i_c = -i_{DC} \quad (11)$$

The pattern (II) of the boost converter can be expressed by the following equations (S is off and D is on) [25];

$$V_{PV} = i_{PV} r_1 + L_1 \frac{di_{PV}}{dt} + E_{DC} \quad (12)$$

$$i_c = i_{PV} - i_{DC} \quad (13)$$

In the pattern (III), the S is off and the diode D becomes reverse biased. To keep the order of the system, this pattern can be described using equations of Pattern (II) by adding the reverse diode resistance to r_1.

The average output voltage is given by;

$$\frac{E_{DC}}{V_{PV}} = \frac{T_{on}}{T_{off}} = \frac{1}{1-D} \quad (14)$$

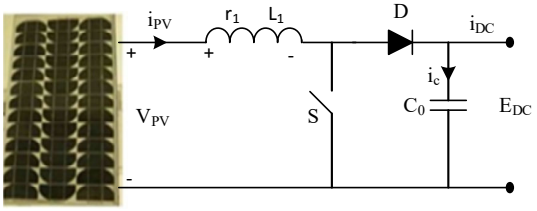

Fig. 2 Boost converter MPPT topology

IV. Proposed Current Based Peak Power Tracking

In this method, the approximately linear relationship between reference maximum power point current (I_{ref}) and the short circuit current (I_{sc}) of the PV array under varying insolation and temperature levels is given by [5]-[6]:

$$I_{ref} = K_1 I_{sc} \quad (15)$$

where; K_1: constant of proportionally which depends on the characteristic of the PV array.

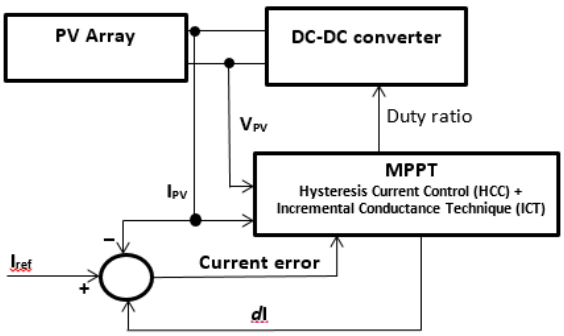

Fig. 3 Proposed MPPT algorithm

Fixed step size will be used which works well under constant irradiance but it has worse behaviors under partial cloudy days [7]. Therefore, the irradiance must be measured to perturb the operation voltage. In this paper, a hybrid hysteresis current control (HCC) and incremental conductance technique (ICT) based maximum power point tracker is designed and implemented to get the benefit from the fast response of the current based tracker, as shown in Fig. 3. The controller loop regulates the PV voltage of the converter and minimizes the error between reference current and the measured current by

adjusting the duty cycle. At changing conditions, a variable of reference value is used, and the reference current is expressed as:

$$I_{ref.new} = I_{ref.old} \pm d\,I \tag{16}$$

where; *dI*: output of incremental conductance control.

V. DTC Principle of Operation

Fig. 4 shows a schematic diagram of a closed loop direct torque control system. The torque command (T^*) is delivered from the PI-speed controller and fed to the torque comparator and compared with the torque developed from the motor. Also, the stator flux command (ψ_s^*) is compared with the actual stator flux (ψ_s). By using three variables (torque error, flux error, and the angle of stator flux position (ϕ_n), the operating point can be obtained [20], [21].

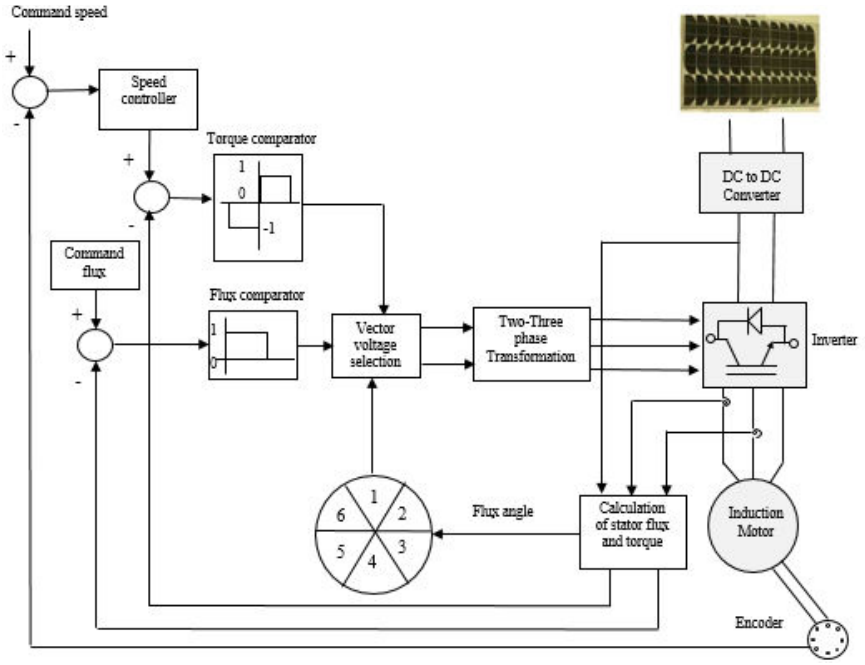

Fig. 4 Block diagram of improved DTC for induction motor drive

A. Inverter Model

The three phase inverter is used with PV system and can be described as follows. To represent the switching state of the inverter, a switching function S_a for phase-a is defined as follow: S_a=1 when upper transistor of phase a is on and S_a=0 when lower transistor of phase-a is off. Similar definitions can be made for phase's b, and c. The phase voltages can be expressed in terms of switching states and the DC link voltage as [20]:

$$V_a = \frac{E_{DC}}{3}(2S_a - S_b - S_c) \tag{17}$$

$$V_b = \frac{E_{DC}}{3}(2S_b - S_a - S_c) \tag{18}$$

$$V_c = \frac{E_{DC}}{3}(2S_c - S_b - S_a) \tag{19}$$

The stator voltage can be expressed in a stationary d-q frame as [20]:

$$V_{ds} = \sqrt{\frac{2}{3}}\left(V_a - \frac{V_b}{2} - \frac{V_c}{2}\right) \tag{20}$$

$$V_{qs} = \frac{1}{\sqrt{2}}(V_b - V_c) \tag{21}$$

The stator currents can be expressed in a stationary d-q frame as [20]:

$$I_{ds} = \sqrt{\frac{2}{3}}\left(I_a - \frac{I_b}{2} - \frac{I_c}{2}\right) \tag{22}$$

$$I_{qs} = \frac{1}{\sqrt{2}}(I_b - I_c) \tag{23}$$

B. Flux Estimation

The simplest and most direct method for determining the stator flux d-q vector requires only the terminal voltage, current, and the stator resistance of the motor. In the stationary d-q reference frame, the stator flux vector and its angle are given by [20],

$$\Psi_{ds} = \int (V_{ds} - R_s I_{ds})dt \tag{24}$$

$$\Psi_{qs} = \int \left(V_{qs} - R_s I_{qs}\right)dt \tag{25}$$

$$\Phi_n = \tan^{-1}\left(\frac{\psi_{ds}}{\psi_{qs}}\right) \tag{26}$$

where; V_s and I_s are the instantaneous space stator voltage and current vector, and R_s is the stator resistance.

C. Torque Estimation

The developed torque of the machine can be obtained by [20];

$$T_d = \frac{3}{2}P(\Psi_{ds}i_{qs} - \Psi_{qs}i_{ds}) \quad (27)$$

VI. Direct Flux and Torque Controller Design

In DTC system under study, constant flux can be obtained by comparing the primary flux with the command flux. The output of the flux comparator will be as follows [20];

$$\varepsilon\,\psi = 1 \quad \text{when } \psi_s < \psi_s^*$$

$$\varepsilon\,\psi = 0 \quad \text{when } \psi_s > \psi_s^*$$

where, ε denote the error signal in both ψ_s. The output of the flux controller is a two levels hysteresis comparator.

The DTC is obtained by adequate selection between active and zero voltage vectors. Hence, when the torque T_d is small compared with T^* it is necessary to increase T_d as fast as possible by applying the fastest vector. On the other hand, when T_d reaches T^* it is better to decrease T_d as slowly as possible. Thus the output of the torque controller can be classified as follows [20];

$$\varepsilon T = 1 \quad \text{if} \quad T_d < T^*$$

$$\varepsilon T = 0 \quad \text{if} \quad T_d = T^*$$

$$\varepsilon T = -1 \quad \text{if} \quad T_d > T^*$$

The output of the torque controller is a three levels hysteresis comparator. The inverter output voltage are given by the outputs of the flux and torque comparators and the angle Φ_n.

VII. Simulation Results

A MATLAB/SIMULINK models has been developed to examine the control algorithms. The controller simulation uses the parameters of an experimental laboratory prototype, which is listed in the appendix. The PV module is made up of 72 multi-crystalline silicon solar cells in series and it provides 150W of nominal maximum power.

The performances of the proposed method have been tested in transient and steady state under identical operation conditions. The possibility of using only forward voltage vectors with zero vectors to obtain positive speed has been tested as well. The following figures show clearly the improvements which can be obtained by the proposals presented in this paper. In the respective simulations, however, only the torque control behavior was investigated. More simulations have been performed considering the flux locus, the torque behavior, stator current, and motor speed.

Fig. 5 shows the response of the system with no load. The transient and steady state flux vector in Fig. 5 (a) shows nearly a circular path indicating a good flux regulation. The electromagnetic torque shown in Fig. 5 (b) is close to the commanded value, while the time taken for the torque reach its commanded value is about 0.3 Sec., ensuring good dynamic torque response. Fig. 5 (c) shows the stator currents in phase a, b and c which are nearly sinusoidal. The motor speed response is shown in Fig. 5 (d). It is clear that the speed reaches to steady state after 0.3 sec.

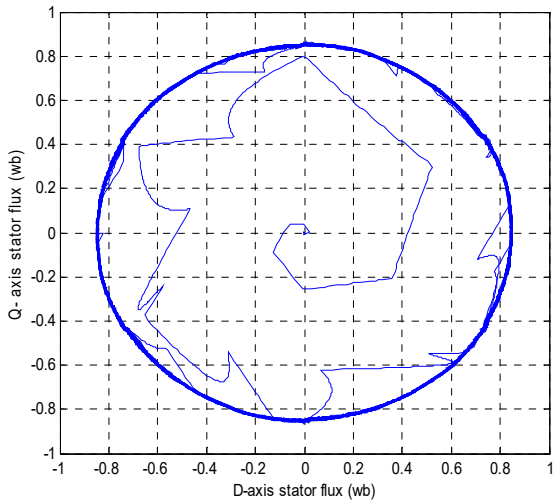

(a)

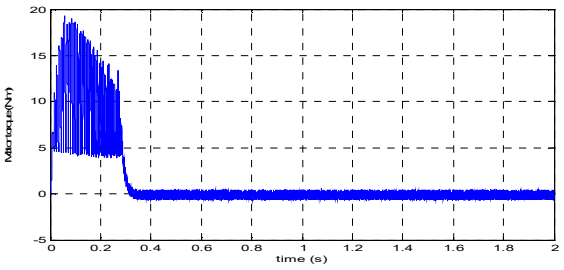

(b)

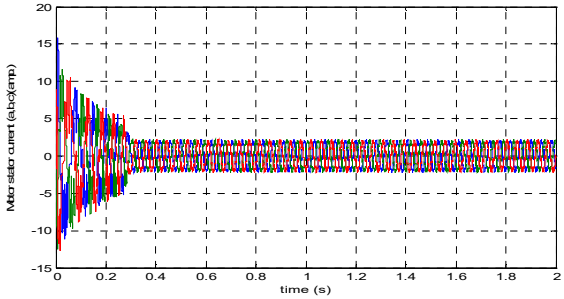

(c)

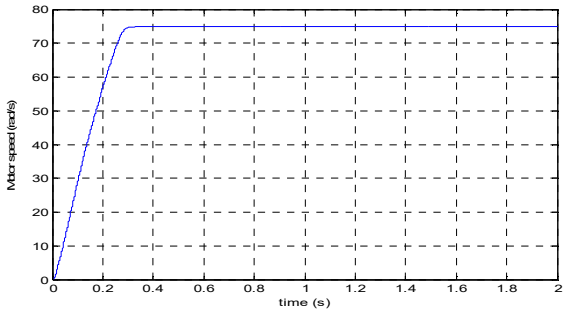

(d)

Fig. 5 Performance of IM under no load (a) d-q stator flux,(b) Developed motor torque (c) Three phase stator motor current (d) Motor speed

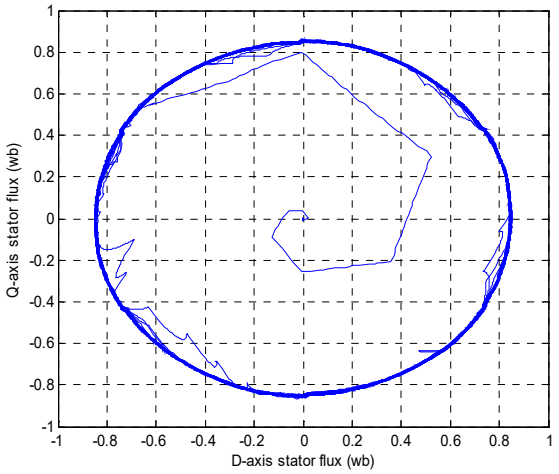

(a)

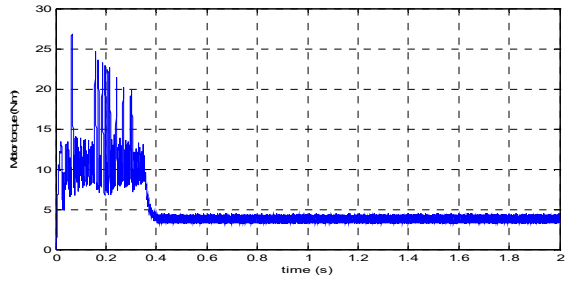

(b)

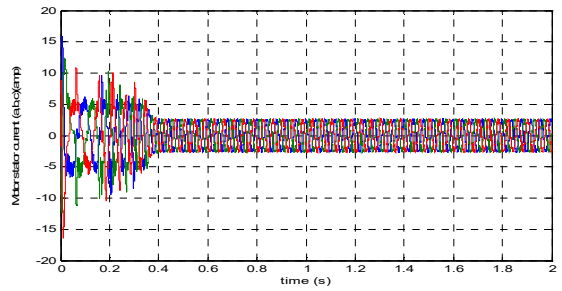

(c)

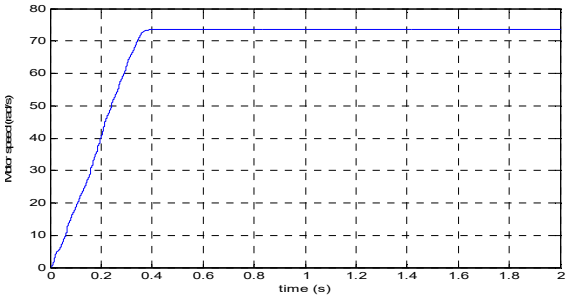

(d)

Fig. 6 Performance of IM under load 4 N.m. (a) d-q stator flux (b) Developed motor torque (c) Three phase stator motor current (d) Motor speed

Fig. 6 shows the response of the system with a torque command of 4 N.m. The transient and steady state flux vector in Fig. 6 (a) shows nearly a circular path indicating a good flux regulation. The electromagnetic torque shown in Fig. 6 (b) is close to the commanded value, while the time taken for the torque reach its commanded value is about 0.4 Sec., ensuring good dynamic torque response. Fig. 6 (c) shows the stator currents in phase a, b and c which are nearly sinusoidal. The motor speed response is shown in Fig. 6 (d).

Fig. 7 shows the response of the system for a step change in torque from 3 N.m. to 7 N.m. keeping the flux command constant. Fig. 7 (a) shows the steady state stator flux, which demonstrates an excellent dynamic flux control under changed command torque. Fig. 7 (b) shows the developed torque which is enclosed to a commanded value of 3 N.m. region or 7 N.m. region. The three phase stator currents are shown in Fig. 7 (c). It is clear that, these stator currents are changed at the instant of changing the command torque and fast retrieve their steady state values. Fig. 7(d) shows the speed response of the system.

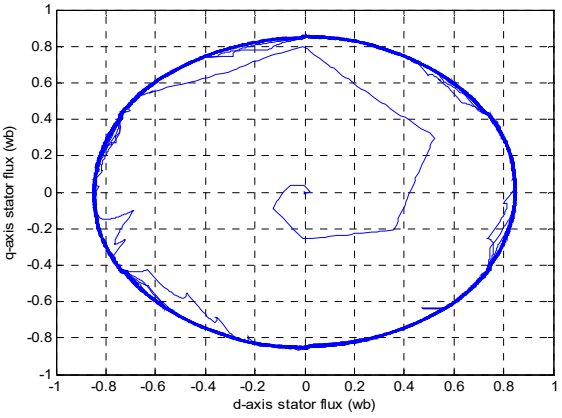

(a)

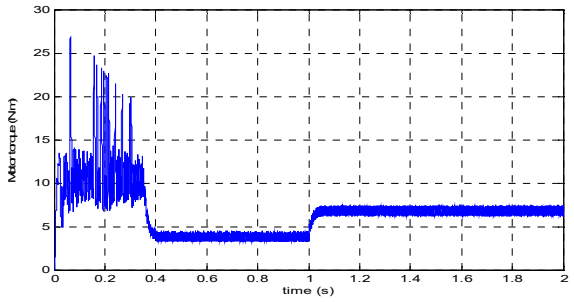

(b)

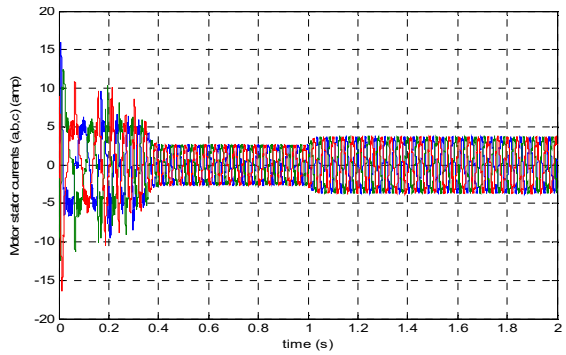

(c)

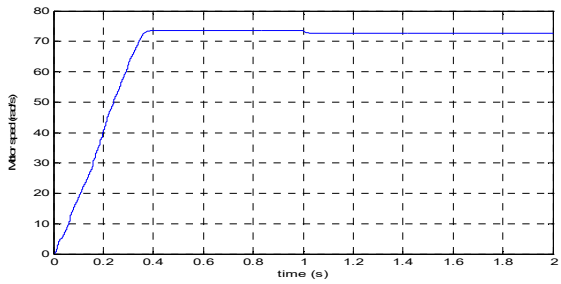

(d)

Fig. 7 Performance of IM under load torque step change (3:7 N.m.) (a) d-q stator flux (b) Developed motor torque (c) Three phase stator motor current (d) Motor speed

Fig. 8 shows simulation results in which a step response of the system is studied at a step change of command torque from 4 N.m. to 7 N.m. at 1.0 Sec., then, at 2.0 Sec. the command torque is decreased to its initial value (4 N.m.). Fig. 8 (a) shows the flux trajectory which has a nearly circular path. Behavior of developed torque shows clearly that the response of the torque is as quickly as possible as shown in Fig. 8 (b). As can be seen from Fig. 8 (c), it is clear that, the stator currents in phases a, b, and c are changing according to the variation of the command torque. Fig. 8 (d) shows the speed response of the system.

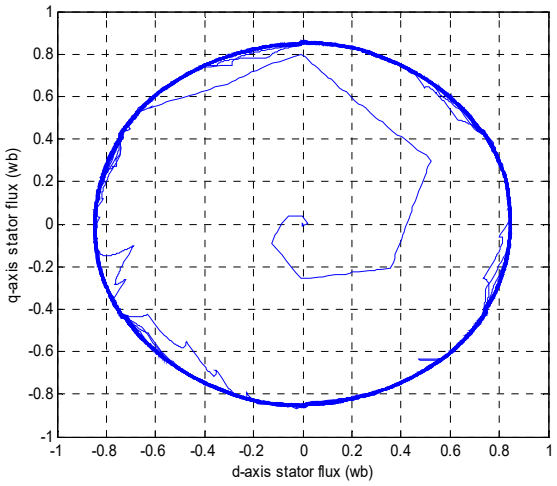

(a)

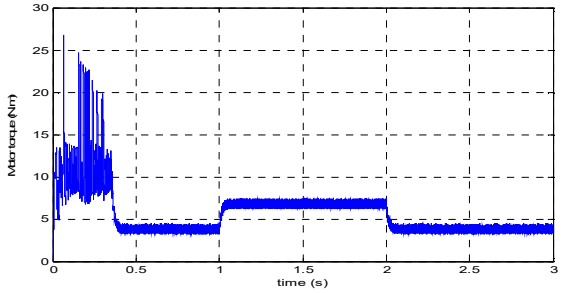

(b)

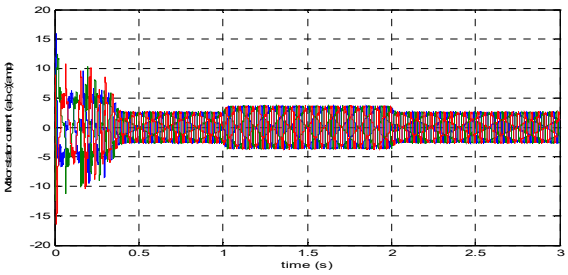

(c)

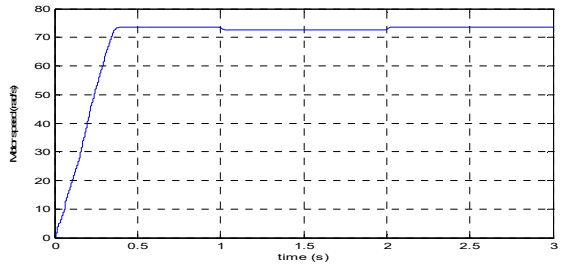

(d)

Fig. 8 Performance of IM under step change in load torque (a) d-q stator flux (b) Developed motor torque (c) Three phase stator motor current (d) Motor speed

VIII. Experimental Results

Experimental implementation of DTC was carried out to verify the behavior of the control system. A three phase, 220 volt, 4 pole induction motor is used. A 50 Amp., 1200 volt IGBT was used as the switching devices in the voltage source inverter. The amplitude of the PV system is 240 volt DC input to the inverter. The two stator currents I_a and I_b are measured by a current sensor and fed to the DSP through A/D converter. Similarly the DC link voltage, which is the output of the boost converter E_{DC} is measured by a voltage sensor, and fed to the DSP through A/D converter. An incremental encoder is coupled to the motor shaft to measure the motor speed. The motor is energized from an inverter bridge, which consists of six IGBT's. This system is fully controlled by using DSP-DS1104 controller board [29], which is installed on a PC computer.

At no load the stator flux command used is 0.8 weber. Fig. 9 (a) shows that the waveform of stator flux in d and q axis is nearly circular which ensure constant flux operation. The torque waveform shown in Fig. 9 (b) has a dc value and the ripple due to the PWM harmonics in the inverter output. Figs. 9 (c)-(f) show the measured stator currents in phase-a, phase-b, phase-c, and compacted three phase - a, b, c which are obtained at no load operation. Fig. 9 (g) shows the motor speed response.

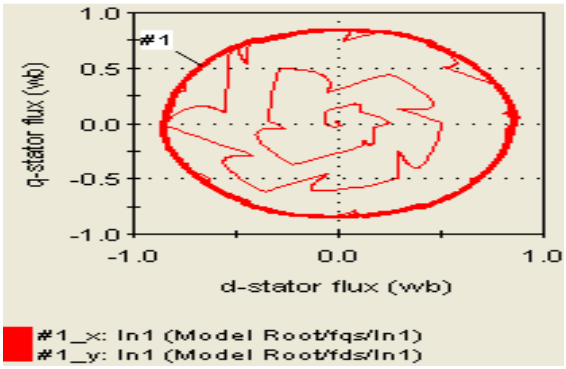

(a)

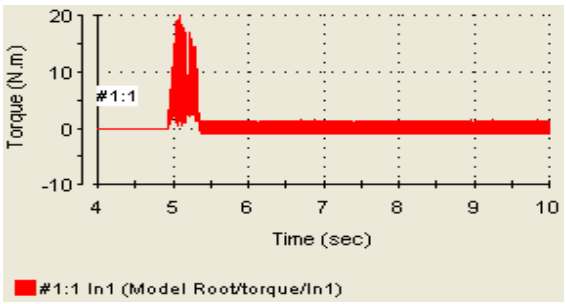

(b)

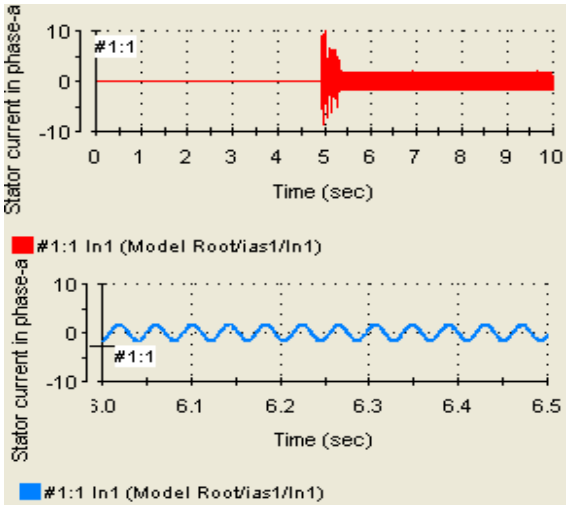

(c)

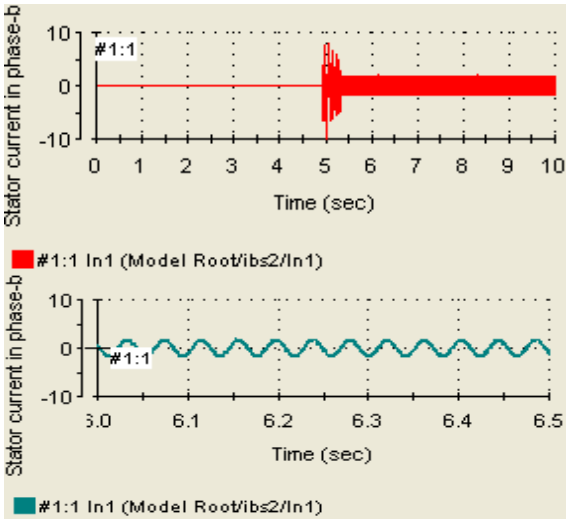

(d)

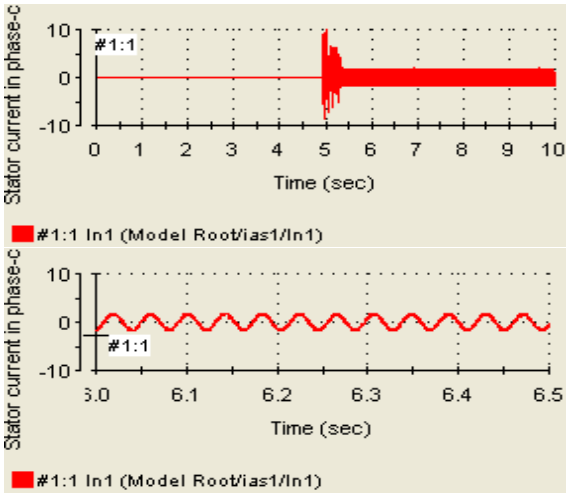

(e)

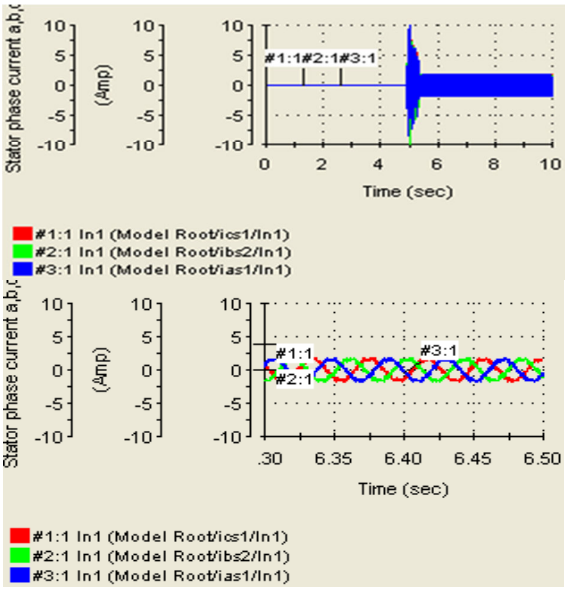

(f)

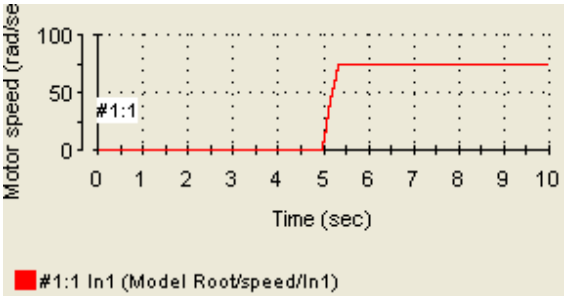

(g)

Fig. 9 Experimental waveforms for DTC fed from PV system at no-load (a) Stator flux in d-q axis (b) Developed torque (c) Stator current in phase-a (d) Stator current in phase-b (e) Stator current in phase-c (f) Three phase stator current in phase a, b, and c (g) Motor speed

Fig. 10 (a) shows that, the waveform of stator flux remains constant along the whole period. Fig. 10 (b) shows the motor developed torque. The ripple and distortion have been attenuated in torque and stator currents waveform. Consequently, the accuracy and efficiency are increased when the motor is loaded. Figs. 10 (c)-(f) show the stator currents in phase-a, phase-b, phase-c, and compacted three phase - a, b, c which are obtained at 3 N.m. constant load operation. Fig. 10 (g) shows the motor speed characteristics.

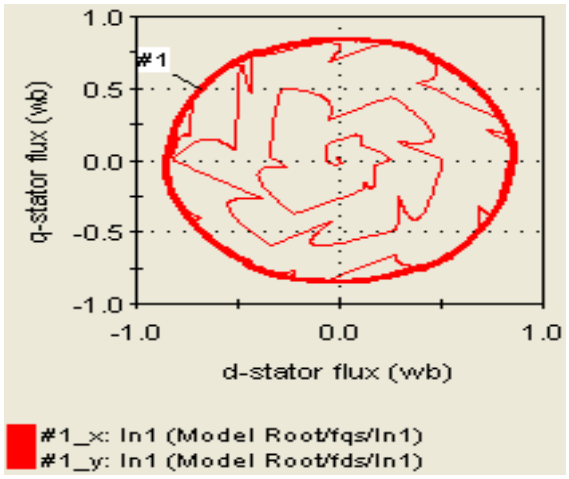

(a)

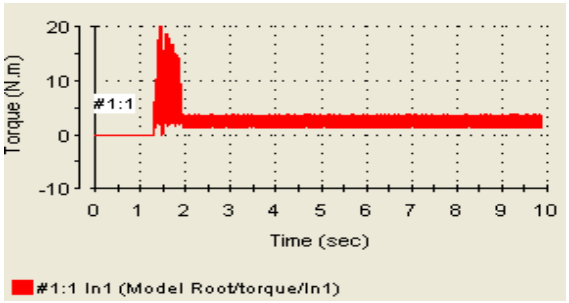

(b)

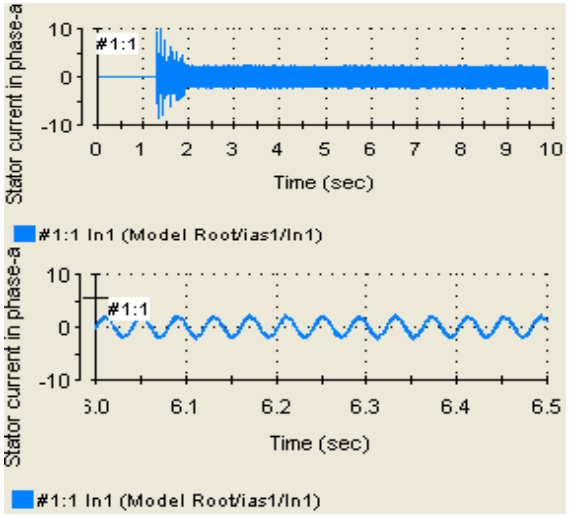

(c)

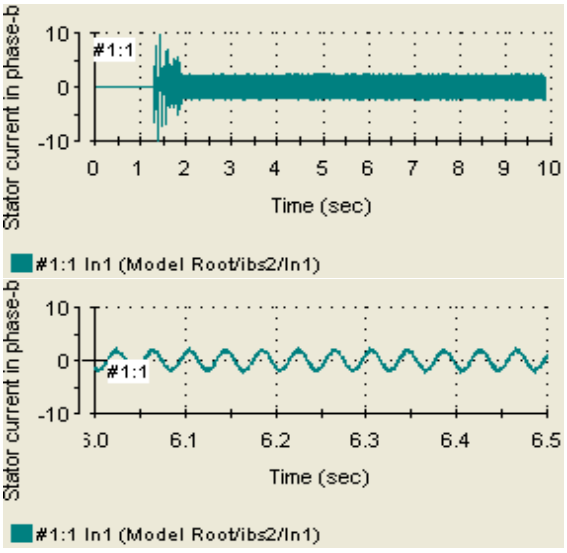

(d)

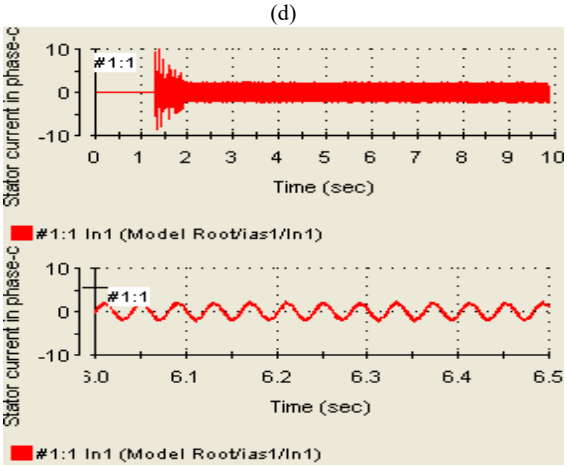

(e)

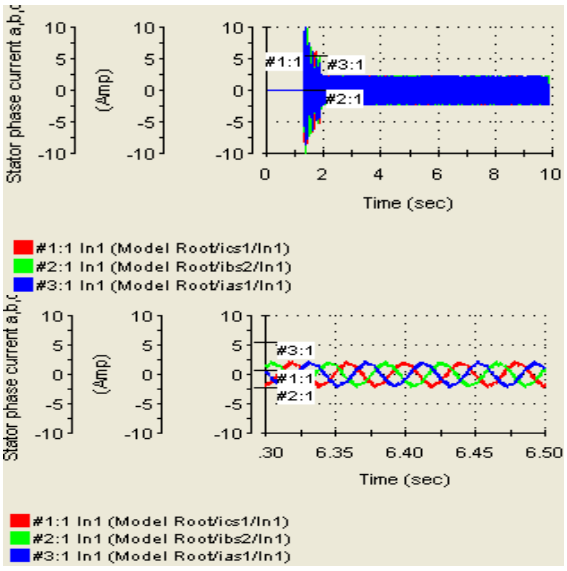

(f)

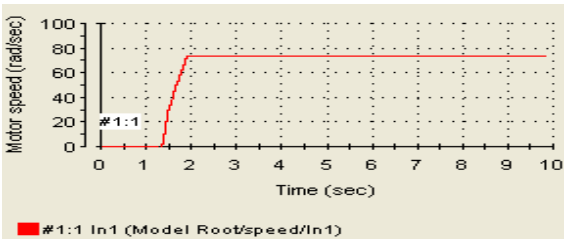

(g)

Fig. 10 Experimental waveforms for DTC fed from PV system at electrical load 3 N.m. (a) Stator flux in d-q axis (b) Developed motor torque (c) Stator current in phase-a (d) Stator current in phase-b (e) Stator current in phase-c (f) Stator current in phase-a, b, and c (g) Motor speed

IX. Conclusion

The presented DTC system supplied from photovoltaic array system can be used in several purposes. Accepted practical system with no need for co-ordinate transformation, voltage, or current decoupling and no need for an encoder is obtained. The result shows that the proposed current based tracker has fast and well damped response. Simulation and experiment results are presented to demonstrate the potential of the proposed scheme. It has been shown that the proposed scheme has several advantages such as, small steady state error, fast response, and small overshoot with disturbance.

Appendix

The induction motor is a three-phase squirrel cage and has the following data:

TABLE I
A THREE-PHASE SQUIRREL CAGE INDUCTION MOTOR DATA

Rated power	1.1 kW
No. of pole pairs	2
Stator resistance	7.4826 Ohm
Rotor resistance	3.6840 Ohm
Mutual inductance	0.4114 Henry
Stator leakage inductance	0.0221 Henry
Rotor leakage inductance	0.0221 Henry
Motor speed	1500 rpm

TABLE II
ELECTRICAL CHARACTERISTICS OF A PV MODULE

Maximum power (P_{max})	180 W
Voltage at Maximum power (V_{max})	35.7 V
Current at Maximum power (I_{max})	5 A
Open circuit voltage ($V_{o.c}$)	44.1 V
Short circuit current (I_{sc})	5.5 A
Rated temperature (T)	298 Kelvin
Number of cells	72 in series

References

[1] G. M. Masters, "Renewable and efficient electric power systems" ISBN 0-471-28060-7, 2004 by John Wiley & Sons, Inc., Hoboken, New Jersey.

[2] Paul A. Lynn, "An introduction to photovoltaics" ISBN 978-0-470-74560-1, 2010 BY John Wiley & Sons Ltd, West Sussex, PO19 8SQ, United Kingdom.

[3] M. G. Wanzeller, R. N. C. Alves, J. V. D. F. Neto and W. A. D. S. Fonseca, "Current Control Loop for Tracking of Maximum Power Point Supplied for Photovoltaic Array," IEEE Transactions on Instrumentation and Measurement, Vol.53, No.4, pp.1304-1310, August 2004.
[4] Rong-Jong Wai, Wen-Hung Wang, and Chung-You Lin, "High-Performance Stand-Alone Photovoltaic Generator System," IEEE Transactions on Industrial Electronics , Vol. 55, No. 1, pp.5-14, January 2008.
[5] J. H. R. Enslin, M. S. Wolf, D. B. Snyman, and W. Swiegers,"Integrated Photovoltaic Maximum Power Point Traking Converter," IEEE Transactions on Power Electronic, Vol. 44, No.6, pp.769-773, December 1997.
[6] H. S. H. Chung, K. K. Tse, S. Y. R. Hui, C. M. Mok and M. T. Ho,"A Noval Maximum Power Point Traking Tracking Technique for Solar Panels Using a SEPIC or Cuk Converter," IEEE Transactions on Power Electronic, Vol. 18, No.3, pp. 717-724, May 2003.
[7] W. Libo, Z. Zhengming, and L. Jianzheng, "A Single-Stage Three-Phase Grid-Connected Photovoltaic System with Modified MPPT Method and Reactive Power Compensation," IEEE Transactions on Power Electronic, Vol. 22, No.4, pp. 881-886, December 2007.
[8] N. Femia,G. Petrone, G. Spagnuolo, and M. Vitelli,"Optimization of Perturb and Observe Maximum Power Point Traking Method," IEEE Transactions on Power Electronic, Vol. 20, No.4, pp. 963-972, July 2005.
[9] M. Veerachary, T. Senjyu, and K. Uezato, "Feed Forward Maximum Power Point Tracking of PV Systems Using Fuzzy Controller," IEEE Transactions on Aerospace and Electronic System,Vol. 38, No. 3, pp.969-981, July 2002.
[10] C.-C. Chu, and C.-L. Chen, "Photovoltaic Cells: A Sliding Mode Control Approach," Journal of Solar Energy, Vol. 83, No. 8, pp.1370-1378, 2009.
[11] F. Boico, and B. Lehman, "Multiple-Input Maximum Power Point Tracking Algorithm For Solar Panels With Reduced Sensing Circuitry For Portable Applications," Journal of Solar Energy, Vol. 86, No. 1, pp. 463-475, 2012.
[12] S. Jain,and V. Agarwal,"A New Algorithm for Rapid Tracking of Approximate Maximum Power Point in Photovoltaic Systems," IEEE Power Electronic Letters, Vol. 2, No.1, pp. 16-19, March 2004.
[13] W. Xiao, W. G. Dunford, P. R. Palmer, and A. Capel, "Regulation of Photovoltaic Voltage," IEEE Transactions on Industrial Electronics, Vol. 54, No.3, pp.1365-1374, June 2007.
[14] T. Esram, J. W. Kimball, P. T. Krein, P. L. Chapman and P. Midya, "Dynamic Maximum Power Point Tracking of Photovoltaic Array Using Ripple Correlation Control," IEEE Transactions on Power Electronics, Vol.21, No.5, pp.1282-1291, September 2006.
[15] E. E. El-Kholy, S. S. Shokralla, A. H. Morsi, and Said A. El-Absawy, "Improved Performance of Rolling Mill Drives Using Hybrid Fuzzy-PI Controller," ELECTROMTION Journal, Vol. 11, No. 4, pp. 213-224, October/December 2004.
[16] M. A. Alhamadi, L. B. Brahim, and S. Tadakuma, "Industrial AC Motor Drives- Status of Technology," in proc. IPEC, Tokyo, Japan, pp. 1219-1224, 2000.
[17] R. Kennel, E. E. El-Kholy, S. A. Mahmoud, A. El-Refaei, and F. El-Kady, "Improved Direct Torque Control for Induction Motor Drives With Rapid Prototyping System," International Journal of Energy Conversion & Management, No. 47, pp. 1999-2010, 2006.
[18] E. E. El-Kholy, M. Abdel-Karim, S. A. Mahmoud, and C. Iung, "Speed Sensor-Less Indirect Field Oriented Control of Induction Motor Without Using Stator and Rotor Resistance," Proceeding of the European Power Electronics Conference (EPE) on Electric Drive Design and Applications, Lausanne, pp. 615-620, October 1994.
[19] U. Baader, M. Depenbrock, and G. Gierse, "Direct Self Control (DSC) of Inverter-Fed Induction Machine A Basis for Speed Control without Speed Measurement," IEEE Transaction Industry Applications, Vol. 28, No.3, pp. 581-588, May/June 1992.
[20] E. E. El-Kholy, S. A. Mahmoud, R. Kennel, A. El-Refaei, and F. El-Kady, "Torque Ripple Minimization for Induction Motor Drives With Direct Torque Control," Electrical Power Components and Systems Journal, Vol. 33, No. 8, pp. 845-859, August 2005.
[21] E. E. El-Kholy, A. EL-Sabbe, A. El-Hefnawy, and Hamdy M. Mharous, "Three Phase Active Power Filter Based on Current Controlled Voltage Source Inverter," International Journal of Electrical Power & Energy Systems, No. 28, pp. 537-547, 2006.
[22] E. E. El-Kholy, A. El-Hefnawy, M. El-Shebiny and Essam A. Wadan, "Design And Analysis of Torque Angle Controller For Induction Motor Drive," Engineering Research Journal, Vol. 24, No. 1, pp. 195-210, January 2001.
[23] G. R. Walker, and P. C. Sernia, "Cascaded DC-DC Converter Connection of Photovoltaic Modules," IEEE Transactions on Power Electronic, Vol. 19, No.4, pp. 1130-1139, July 2004.
[24] N. Kasa, T. Iida, and L. Chen, "Fly back Inverter Controller by Sensor less Current MPPT for Photovoltaic Power System", IEEE Transactions on Industrial of Electronics, Vol.52, No.4, pp.1145-1152, August 2005.
[25] J. L. Duran-Gomez, E. Garcia-Cervantes, D. R. Lopez-Flores, P. N. Enjeti, and L. Palma, "Analysis and evaluation of a series-combined connected boost and buck-boost dc-dc converter for photovoltaic application," Twenty-First Annual IEEE Applied Power Electronics Conference and Exposition (APEC '06), pp. 7, 2006.
[26] A. Z. A. Firdaus, M. Normahira, K. N. Syahirah, and J. Sakinah, "Design and simulation of Fuzzy Logic Controller for boost converter in renewable energy application," IEEE International Conference on Control System, Computing and Engineering (ICCSCE), pp. 520-524, 2013.
[27] F. Kurokawa, K. Ueno, and K. Murata, "Performance characteristics of digital control boundary current mode DC-DC converter,"15th International Conference on Power Electronics and Motion Control Conference (EPE/PEMC), 2012.
[28] Akihiro Oi, "Design and simulation of photovoltaic water pumping system," Msc. dissertation, Dept. Electrical Eng., Univ. California polytechnic state, 2005.
[29] DSP-CIT Hardware, "dSPACE digital signal processing and control engineering" GmbH, Germany, 1993.

E. E. El-Kholy, was born in Menoufiya, Egypt in 1963. He received his B.Sc., and M.sc. degree in Electrical Engineering from Faculty of Engineering, Menoufiya University in 1986, and 1992 respectively. From January 1993 to January 1996 he was Ph.D. student at the I.N.P.L., Nancy University, France, under an academic channel exchange program. He received his Ph.D. degree in 1996. He was a visiting research fellow to I.N.P.L., Nancy University, France during summer 1997. He was a visiting professor to Electrical Machines and Drives Dept., Wuppertal University, Germany during August 2001 to January 2002. He joined the Department of Electrical Engineering, Faculty of Engineering, Menoufiya University as a demonstrator in 1986. Then, he became an assistant lecturer in 1992 and was appointed as an assistant professor in 1996. In July 2002, he was appointed as an associating professor. In July 2006, he was appointed as a professor. His main professional interests include AC and DC drives, Renewable Energy, direct torque and field oriented control techniques, DSP control and Power Electronics. He has published several technical papers in these areas.